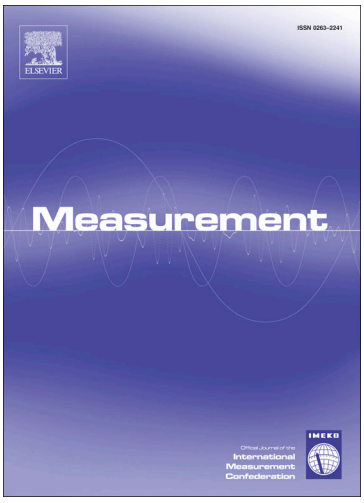

Characteristics of shunting effect in resistance spot welding in mild steel based on electrode displacement

Bobin Xing, Yi Xiao, Qing H. Qin

PII: S0263-2241(17)30684-X
DOI: https://doi.org/10.1016/j.measurement.2017.10.049
Reference: MEASUR 5051

To appear in: *Measurement*

Received Date: 15 June 2017
Revised Date: 16 October 2017
Accepted Date: 24 October 2017

Please cite this article as: B. Xing, Y. Xiao, Q.H. Qin, Characteristics of shunting effect in resistance spot welding in mild steel based on electrode displacement, *Measurement* (2017), doi: https://doi.org/10.1016/j.measurement.2017.10.049

Characteristics of shunting effect in resistance spot welding in mild steel based on electrode displacement

Bobin Xing, Yi Xiao, Qing H. Qin *
Research School of Engineering, Australian National University, Acton, ACT 2601, Australia

* Corresponding author

Email address: Qinghua.Qin@anu.edu.au; Fax: (+61 2) 6125 5476

Abstract

Shunting effect of resistance spot welding is evaluated based on the electrode displacement signals. The shunted welds in mild steel with different weld spacing were produced. The results showed that the weld spacing and nugget diameter were polynomial-correlated, and the minimum welding spacing of 20 mm can be derived from the results. Both the peak value and gradient of electrode displacement in the weld stage indicated strong correlations with the nugget diameters of shunted welds. Additional shunt path was found to further aggregate the shunting, suggesting the decline in the values of profile features. Furthermore, it is found that the shunting effect led to the decline of the dynamic resistance curves, which is contradictive to the trends between acceptable-sized and undersized welds claimed based on the single weld study. The paper shows that electrode displacement curves of shunting can be incorporated into existing quality monitoring system.

Keywords: Resistance spot welding; Shunting; Electrode displacement

1. Introduction

Resistance spot welding (RSW) has extensively been applied to metal sheet assembly in the automobile industry. In the manufacturing of a body-in-white (BIW) structure, many spot welds are continuously produced within the same region of a component, where the problems of shunting and poor fit-up are inevitable. As a parallel electrical path from the existing weld (shunt weld) is formed, the welding current flowing to the new weld (shunted weld) is reduced, as shown in Figure 1. The insufficient generation of heat caused by shunting adversely influences the strength and nugget diameter of the shunted weld. This, together with poor fit-up problem introduced by existing welds, narrows the weldability lobe and leads to expulsion [1].

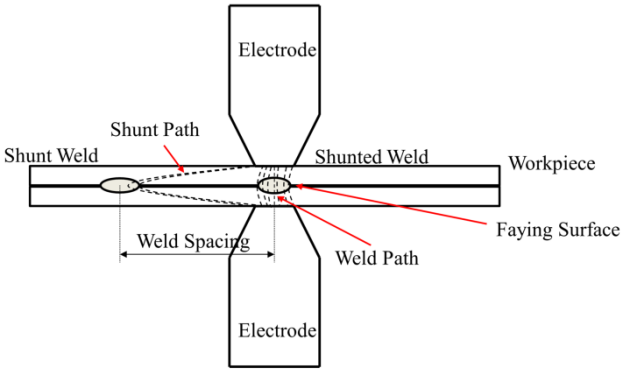

Figure 1 Schematic diagram of single shunting

Researchers have carried out experimental studies on shunting effect of RSW in various metals [2-4]. Wang investigated effects of some experimental parameters on shunting and derived an analytical equation for shunting in mild steel [2], from which critical minimum weld spacing for mild steel under various conditions was evaluated. Wang found that the contact resistance at the faying surface substantially affects the critical minimum welding spacing, as the consequent low electrode force and high contact resistance aggregate shunting. He also pointed out that darker and larger impression mark presented in shunted welds, which could be considered in the visual inspection of weld quality. On the other hand, it was found that the low electrical resistivity of aluminium makes it vulnerable to shunting effect [4]. The use of increased current, instead of increased weld spacing, is more effective in solving shunting problem in aluminium alloy.

Due to the complexity of the thermo-mechanical-electrical phenomenon in RSW, some numerical studies have been conducted for the understanding of the shunting problem in Al sheets [5-9]. A good agreement is reached between the simulated nugget diameters and the measured ones. Moreover, the simulated current density for the shunted weld is proportional to the weld spacing. A heat compensation mechanism was revealed in multi-spot welds, as the shunted weld was heated by electrical current and temperature risen in the base materials due to the previous welds [5]. However, the existing studies modelled the shunting without the consideration of any workpiece deformation, and physical properties of base materials were simplified. Direct incorporation of the numerical modelling result for shunting prediction seems difficult.

In the production environment, it is crucial to utilise dynamic signals to monitor weld quality and thus develop a feedback control system [10,11]. Electrode displacement (ED) has been extensively used to characterise the weld quality in a range of existing studies, via the techniques of image-process [12-14], non-contact laser displacement sensor [15,16] and contact-type displacement sensor [17,18]. ED curve describes the thermal expansion of sheets in the weld stage, where a range of factors affect the features of curves, such as surface conditions of the sheets [19], welding parameters [20] and electrode degradation [21]. Jou revealed the relationship between the profile features, such as peak value and ED velocity,

and nugget diameter in an array of steels [20]. Some characteristics in ED signals are found to be strongly related to phase transformation in the fusion zone and the contact condition. Image based electrode displacement showed a good accuracy over the conventional displacement sensor, in which the thermal expansion in electrodes was properly considered [12]. Zhang conducted a case study on shunting problem based on the ED signals with varied number of shunt welds and weld spacing [17]. A clear difference in the signals was observed among shunt and shunted welds, which aligned with the difference between acceptable sized welds and undersized welds. On the other hand, the relationship developed for the tensile-shear strength (TSS) and profile quantities from the dynamic resistance (DR) curves was found to contradict the trends observed in shunting [22,23]. Likewise, the electrode vibration signal processed from ED accurately estimated the nugget diameters of the shunted welds [24]. In such case, the vibration signal of double shunted weld showed different signal characteristics over the single shunted weld and the shunt weld. However, some key features in the vibration signals disappeared in the case of severe shunting.

A reliable online monitoring system on shunting is assumed to be able to estimate the nugget diameter of shunted weld based on the weld spacing and number of existing welds. To the author's best knowledge, limited work has been done to quantitatively determine nugget diameter affected by shunting in RSW. Here, electrode displacement is proposed to characterise the shunting problem with respect to different weld spacing and the number of shunt weld. To demonstrate the effectiveness of the method, the actual nugget diameters at various shunting conditions are measured after standard metallurgical procedures and the relationship between nugget diameter and profile of electrode displacement is established. The present work provides an insight into constructing a viable online monitoring system for weld quality subjecting to shunting effect in RSW.

2. Experimental Procedure

2.1 Experiment layout and material

The experiments were conducted on a single-phase AC DN-50 pedestal welder. The frequency of AC source was 50 Hz. The base material was 1-mm-thick cold rolled steel CA2S-E, whose chemical composition and material properties are listed in Table 1 and 2, respectively.

Table 1 Chemical composition of CA2S-E (wt %)

Material	C	Si	S	P	Mn	Al
CA2S-E	0.04 – 0.07	0.005 – 0.01	0.008 – 0.02	0.005 – 0.02	0.18 – 0.25	0.03 – 0.05

Table 2 Mechanical properties of CA2S-E

Material	Yield Strength (MPa)	Ultimate Tensile Strength (MPa)	Elongation (%)
CA2S-E	160 – 250	270 – 340	34 – 46

Figure 2 presents the layout of the electrode displacement measurement. The measurement system comprised an objective beam, a MICRO-EPSILON non-contact laser displacement sensor (optoNCDT 1402-5) and a signal acquisition device. The sensor fixture and the objective beam were made of engineering plastic, which had an appealing combination of mechanical strength and the resistance to thermal expansion. The laser displacement sensor has a resolution of 1 μm, capable of probing the movement of the electrode due to thermal expansion of the nugget. Welding current I_w and welding voltage U_w were acquired for dynamic resistance computing. The sampling frequency of the signal was 10 kHz. Dynamic resistance R_{RMS} per half cycle is calculated using equation (1):

$$R_{RMS}=\frac{U_{RMS}}{I_{RMS}} \tag{1}$$

where U_{RMS} and I_{RMS} are the effective voltage and current every half cycle, respectively.

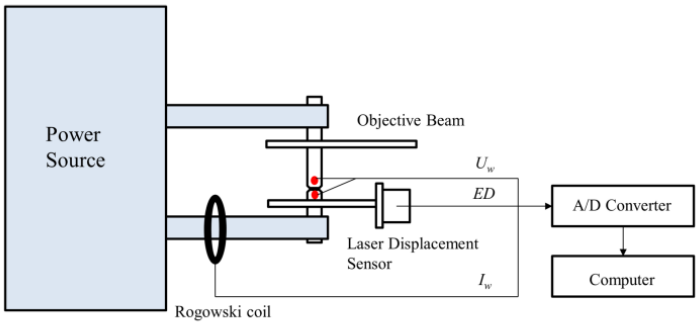

Figure 2 Schematic diagram of experimental set-up

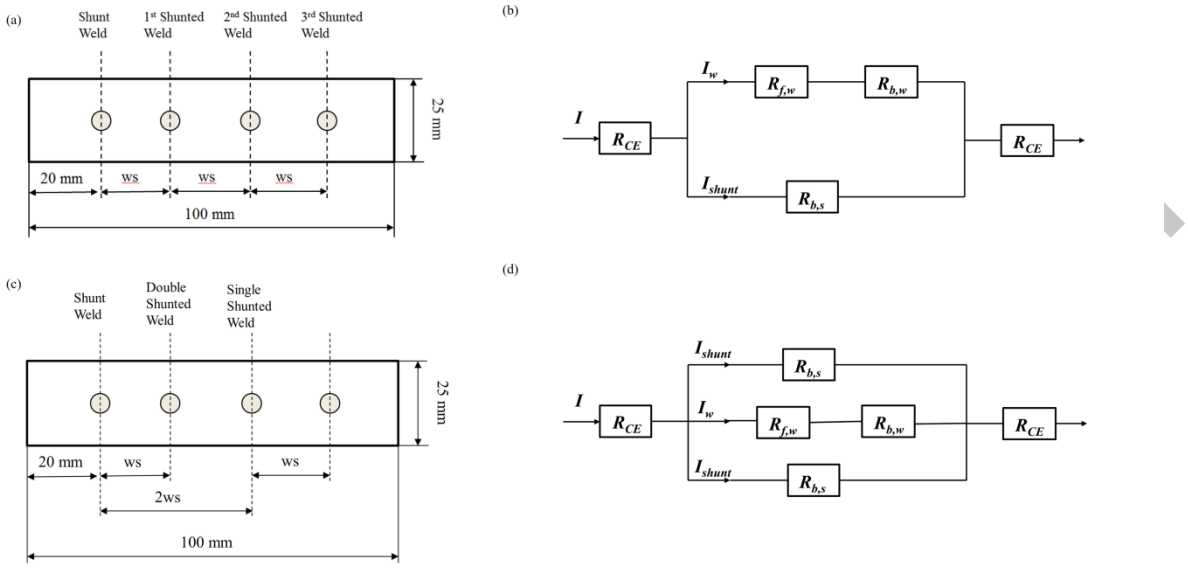

Figure 3 Schematic diagram of welding sequence applied. (a) Single shunting. (b) The equivalent circuit for single shunting. (c) Double shunting. (d) The equivalent circuit for double shunting.

Spot welds were made in the arranged sequences shown in Figure 3 (a) and (c), with altered weld spacing (*ws*). These two distinct weld sequences created single shunting and double shunting, respectively. Shunted welds were named after the order of the production sequence; thus, the shunted welds next to shunt welds were referred as first shunted welds, and the shunted welds next to the first shunted welds were known as second shunted welds. A similar naming was also applied to double shunted welds. In addition, the equivalent circuits of single shunting and double shunting are presented in Figure **3** (b) and (d). The welding current I_w and shunting current I_{shunt} in single shunting are calculated by

$$I_w = \left(\frac{R_{b,s}}{R_{b,s}+R_{b,w}+R_{f,w}}\right)\cdot I \tag{2}$$

$$I_{shunt} = \left(\frac{R_{b,w}+R_{f,w}}{R_{b,s}+R_{b,w}+R_{f,w}}\right)\cdot I \tag{3}$$

I is the overall welding current flowing from the electrode. $R_{b,s}$ is the bulk resistance of the shunting path, and $R_{b,w}$ is the bulk resistance at the welding path, and $R_{f,w}$ is the contact resistance at the faying surface. $R_{b,s}$ is found to be inversely proportional to weld diameter of the shunt and shunted weld and proportional to weld spacing and the thickness of the sheet; while $R_{b,w}$ and $R_{f,w}$ are proven to be independent to weld spacing [2]. The problem is simplified by assuming $R_{b,s}$ for shunting path is identical in double shunting. Thus, the equivalent equation of I_w of double shunting is derived:

$$I_w = \left(\frac{\frac{1}{2}R_{b,s}}{\frac{1}{2}R_{b,s}+R_{b,w}+R_{f,w}}\right)\cdot I \tag{4}$$

where $\frac{1}{2}R_{b,s}$ is the equivalent bulk resistance for two parallel shunt welds. When the ratio $(R_{b,w}+R_{f,w})/\frac{1}{2}R_{b,s}$ increases, the portion of the shunting current I_{shunt} simultaneously increases.

The weld parameters to identify the appropriate welding current for welds with acceptable quality are listed in Table 3. Each weld sequence was repeated for three times with the optimal welding current. The time interval between two adjacent welds was 15 s. Truncated cone Cu-Cr-Zr electrodes with a tip diameter of 6 mm were used. Before measuring signals on shunted welds, an electrode conditioning was implemented on the 1-mm-thick mild steel. According to Hu's work, it is necessary to eliminate the dynamic behaviour in joint strength of a new pair of electrodes [25]. Welding parameters in the electrode conditioning included welding current of 8.8 kA, electrode force of 2.7 kN and a welding time of 0.2 s. The electrode conditioning was carried out until consistent electrode displacement values were achieved for the last ten welds.

Table 3 Welding parameters used in this study [26,27]

Current (kA)	Time (ms)	Electrode Force (kN)	Weld Spacing (mm)
7.2,8.8,10.4	200	2.7	8, 12, 15, 24, 30

The nugget diameters of the shunt and shunted welds were measured via the standard metallurgical procedure. 4% nital solution was used for etching to reveal the nugget and heat affected zone (HAZ). The diameters of the nuggets were measured under a stereomicroscope.

2.2 Electrode displacement signal analysis and processing

The examples of the original and de-noised ED signals are demonstrated in Figure 4. The electrode displacement occurred in three stages: squeeze, weld and hold. ED signals were collected when two electrodes were in contact during the squeeze stage. The signal saw no fluctuation in the squeeze stage. In the weld stage, the welding current flowed through the base materials, and base metals started to melt induced by joule heating. The thermal expansion and solid-to-liquid phase transformation collectively account for the total electrode displacement in the weld stage. A strong vibration was found to accompany the elevated displacement, caused by the AC power source. It is similar to the vibration reported in Wang's work [28]. The frequency of the oscillating signal of the electrode displacement was around 100 Hz, which is twice of that for the spot welder. Electrode force was applied to the steel at the hold stage. The molten metal experienced a rapid cooling through the water-cooled electrodes, resulting in gradual decline in ED. Such collected signal was further processed through a low-pass filter to eliminate the frequency components from electrode vibration. The de-noised signal shown in Figure 4(a) precisely describes the equivalent electrode displacement.

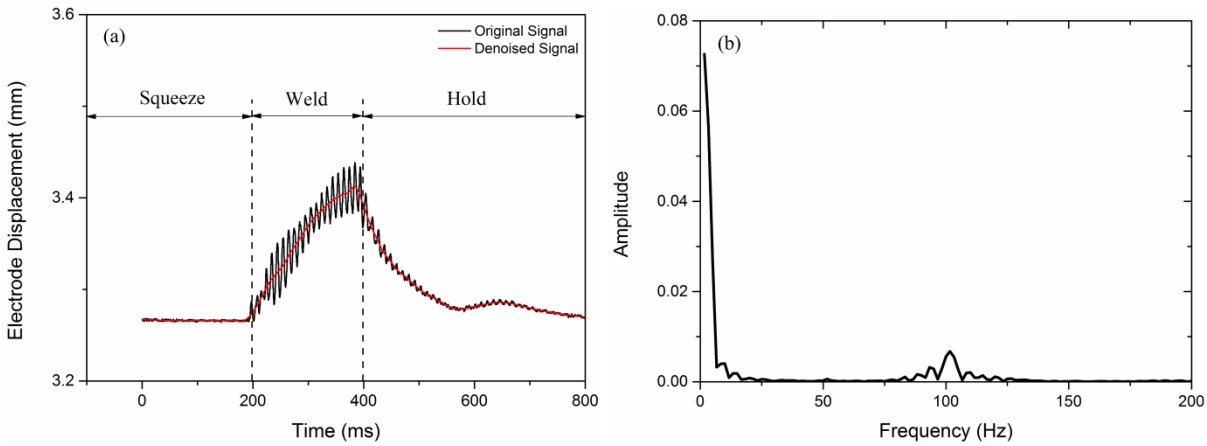

Figure 4 (a) Electrode displacement in the time domain. (b) Frequency spectrum of electrode displacement

3. Results and discussion

3.1 Effect of welding current on electrode displacement

Shunting effect is known as a phenomenon in which welding current for a new weld is diverted by existing welds in the same area. It is important to determine in advance the welding current used for producing shunt welds.

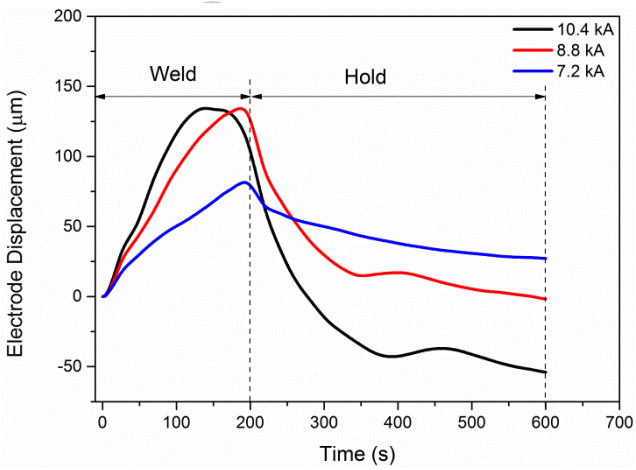

Figure 5 The effect of welding current on electrode displacement

The electrode force of 2700 N and the welding time of 200 ms were used. Cold weld was produced with welding current of 7.2 kA, while good weld was produced with welding current 8.8 kA. Welding current of 10.4 kA was the upper limit without any expulsion. Figure 5 demonstrates the ED signals with different welding current levels. Significant variances in ED profiles were seen. The lowest peak value was seen in the ED curve for a cold weld, which had a gentle slope in the weld stage. And the base materials began to melt and form a nugget, but the heat input was not sufficient for yielding an adequately sized nugget. When an acceptable sized weld was made, a much higher ED peak value was generated and a moderate electrode velocity was achieved. However, no considerable increase in peak value was found for the welding current from 8.8 kA to 10.4 kA. Further thermal expansion was

constrained by the limited electrode geometry [18]. Therefore, the value of displacement did not further climb. On the other hand, the ED velocity with welding current of 10.4 kA outperformed those at lower current levels, as the greater amount of Joule heat was generated by:

$$P=I^2R \tag{5}$$

where I is the welding current, R is the total resistance. Expulsion is likely to occur if an excessive amount of welding current is used. It weakens mechanical performance of the nugget and aggregates electrode degradation [29]. To investigate the shunting effect, welding current of 8.8 kA was used in the succeeding welding experiments.

It is worth mentioning that a considerable difference of ED signals in the hold stage was found with respect to different spot weld qualities. Such differences in ED signals can be explained with two methods. Firstly, Lai investigated the effect of the indentation mark depth on the weld strength, where the indentation depth was measured by the difference between the starting point and end point of the ED signal [30]. He found the indentation depths of cold weld and expulsion usually sit outside the acceptable range of weld size. However, the values in this study were found to be much smaller than those established in Lai's study. Hence, the endpoint value in this study may not accurately reveal the indentation mark. Alternatively, Jou suggested the ED signals in the hold stage reflect solid-state phase transformation [20]. As the level of heat generated was increased, an adequate volume of liquid metal was preserved at the faying surface. When the welding current was terminated, the electrodes clamped on the base material while the molten metal experienced a rapid cooling via the water-cooled channel on the electrodes. The heat input determines the size of fusion zone, thus causes the volume change in the hold stage.

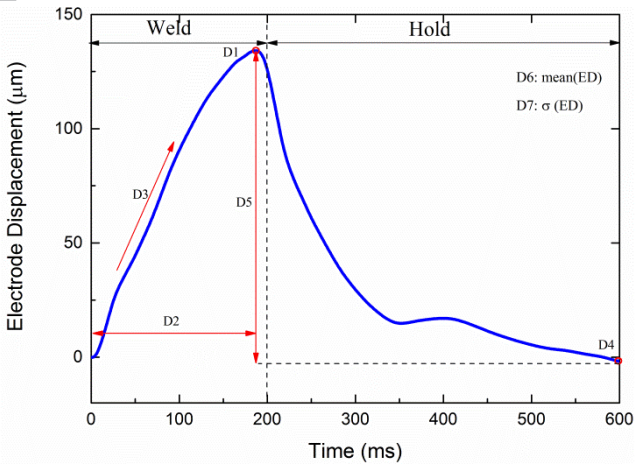

Figure 6 Electrode displacement profile quantity extraction in time domain

Seven profile quantities with physical meanings were extracted from the ED signal in the time domain, shown in Figure 6. D1, D2, D3 correspond to the peak value in ED, the location of ED peak and ED velocity. D4 and D5, on the other hand, reflect the endpoint value of the

ED signal and the overall decline between D1 and D4. Lastly, D6 and D7 are the mean value and standard deviation of the ED signal, respectively.

3.2 Effect of welding spacing on electrode displacement

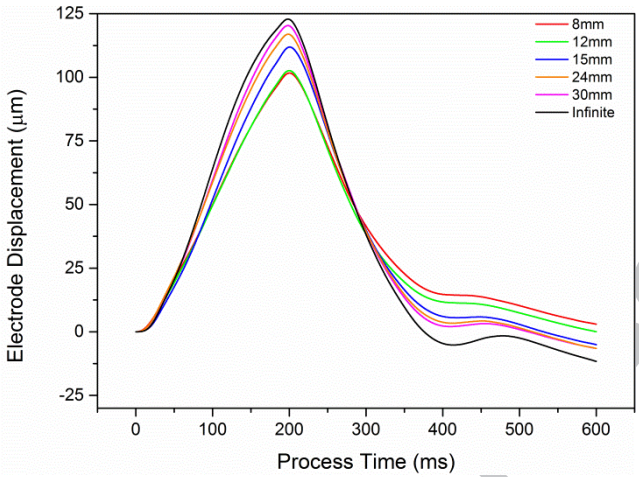

Figure 7 Electrode displacement of the single shunted welds at different weld spacing.

The ED signals of averaged first shunted weld at different weld spacing are summarised in Figure 7, where the weld spacing ranges from 8 mm to 30 mm. It is noted that with the decline of the weld spacing, the peak values of the ED signals shifted downward while the slopes of the ED in the weld stage proportionally decreased. The shunting path substantially diverted the welding current, resulting in small thermal expansion and gentle electrode displacement velocity for shunted welds. Figure 8 shows the longitudinal sectional views of the nuggets on various welding spacing. The nugget diameters for shunt welds were nearly identical. Due to the shunting effect, it is found that the nugget diameter of shunted weld was substantially reduced from shunt weld with weld spacing of 8 mm, while the decrease in nugget diameter was less evident with larger weld spacing. The relationship between the weld spacing and the nugget diameter of tested samples is shown in Figure 9. They were fitted with a polynomial curve, similar to that in Bi's work [4]. It is known that the acceptable minimum nugget diameter should exceed $5\sqrt{t}$, where t is the thinnest thickness of base materials. The approximate minimum weld spacing is found to be around 20 mm, as demonstrated in Figure 9. In addition, the indentation marks in shunted welds for different spacing did not distinctly vary in Figure 8, usually around ~150 μm. The indentation depths in Figure 7 were ~ 10 μm, calculated based on Lai's work, which does not reflect the actual indentation mark [30].

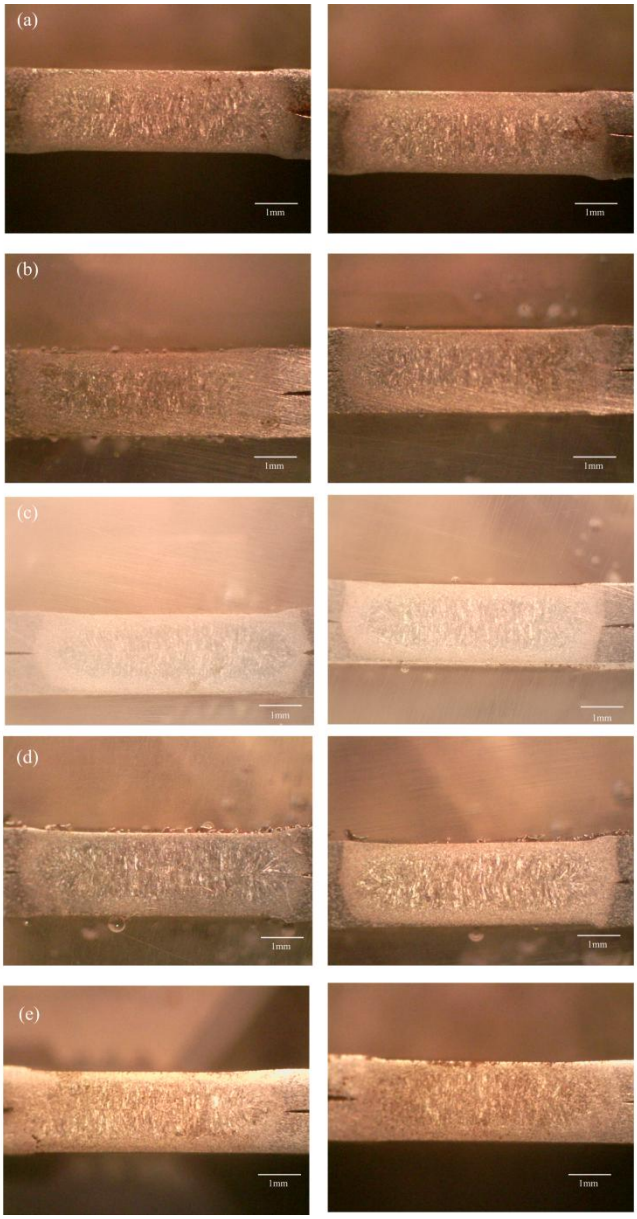

Figure 8 Longitudinal-sectional views of shunt welds and first single shunted welds. a) 8 mm. b) 12 mm. c) 15 mm. d) 24 mm. e) 30 mm

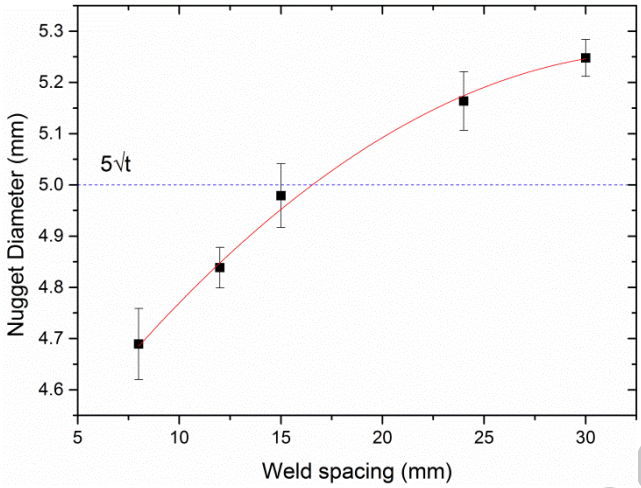

Figure 9 Nugget diameters of the first single shunted welds with different weld spacing

The seven ED profile quantities (D1 – D7) with respect to nugget diameters are presented in Figure 10. Some of them (D1, D3, D5 and D7) show strong correlations to the nugget diameter, whereas D4 displays an inverse polynomial correlation to nugget diameter. The trends developed among D1, D3, D5 and D7 are similar to each other. D1 and D3, known as the ED peak and ED velocity, are strongly related to the overall magnitude of thermal expansion and the rate of thermal expansion. Both of them play a key role in nugget nucleation and development. Not much work presented focus on the ED in the hold stage, since the thermal expansion ceases and the molten metal gradually solidifies at this stage. Nonetheless, the indentation mark and liquid-to-solid phase transformation occur at the hold stage. D5, dependent to D1 and D4, is used to describe the solidification of the fusion zone. A strong relationship is found among the shunted welds in D5, where the volume changes in solidification at the hold stage determines the relative nugget diameter. Pouranvari disclosed the strong correlation of indentation depth and nugget diameter at various heat inputs [31]. The indentation depth manifested in his study shows a polynomial correlation against the heat input, matching the curves fitted for D4 and D5. On the other hand, D2, the time of ED peak, does not exhibit any linear relationship with the nugget diameter. However, it is worth noting that the shunted welds that exceed the minimum nugget diameter attain lower D2 values than those of the undersized welds. Shunt welds with sufficiently large weld spacing result in a significant variance in ED values due to thorough thermal expansion and solidification. Thus, D7, the standard deviation of ED, is related to the nugget diameter. Lastly, the mean value (D6) fluctuates with different weld spacing, making it less useful in detecting shunting problem. Three profile quantities, namely D1, D3 and D7, can be considered for shunting detection.

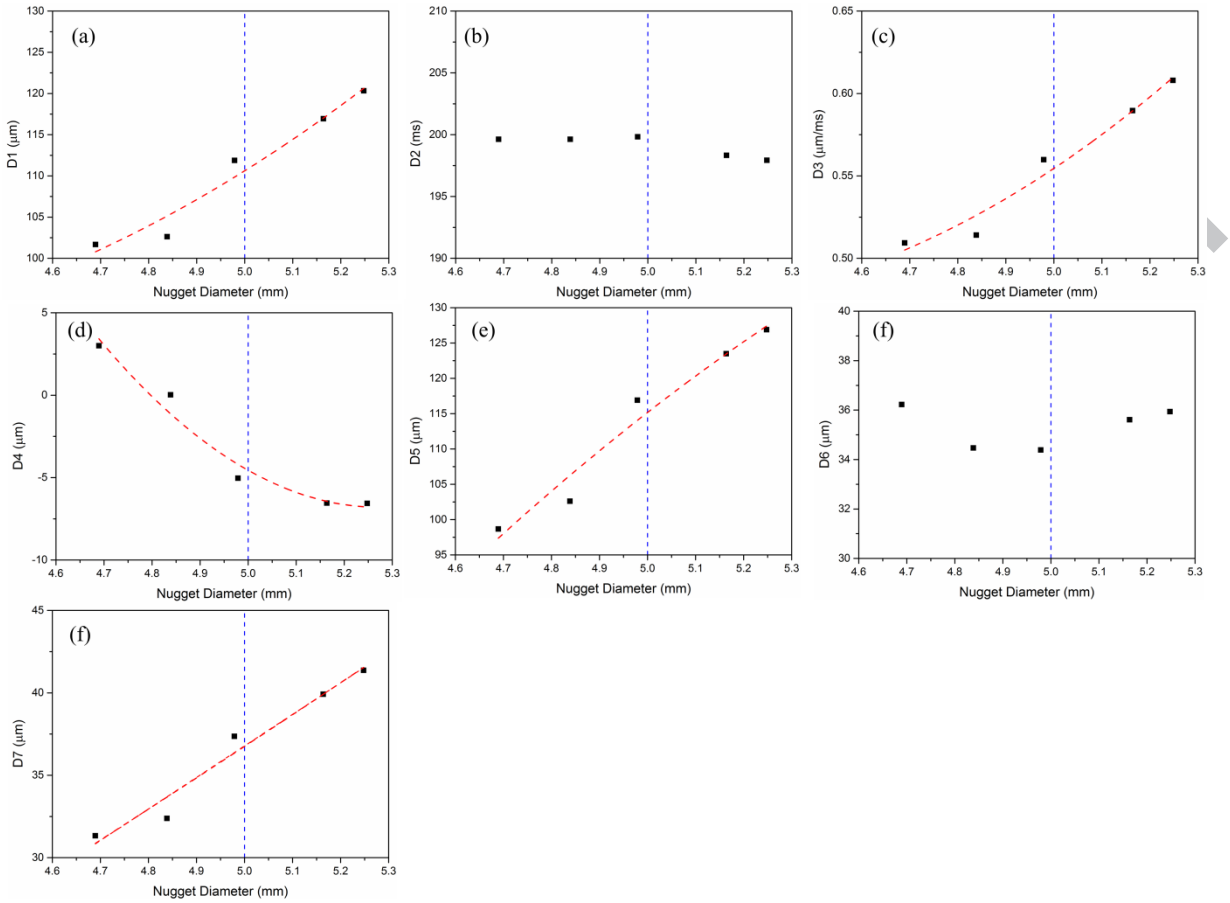

Figure 10 Profile Quantities on ED signals and nugget diameters with different weld spacing.

3.3 Effect of number of shunted welds on electrode displacement

Figure 11 presents the impact of double shunting on electrode displacement signals. Single shunting and double shunting were implemented via the welding sequences shown in Figure 3, with the welding spacing of 8 mm and 15 mm. The double shunting from existing welds led to a significant decline in the peak values of ED curves illustrated in Figure 11 (a) and (b). Their peak values in ED curves with 8 mm weld spacing are lower than those with 15 mm.

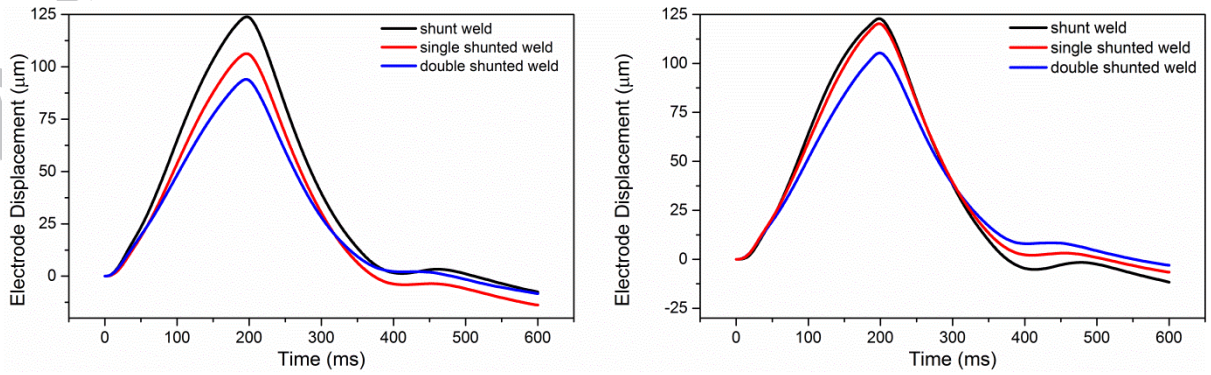

Figure 11 Electrode displacement of varied number of shunted welds with weld spacing of (a) 8mm and (b) 15mm

Figure 12 demonstrates some cross-sections of double shunted welds. It can be seen that the shape of double shunted welds (2nd) were affected by the existing welds (1st and 3rd). The outline of double shunted weld was more rectangular than elliptical as that of the shunt weld. The nugget diameters of welds are demonstrated in Figure 13. None of double shunted weld met the minimum nugget diameter. Hence, the critical double shunting distance should be beyond 15 mm.

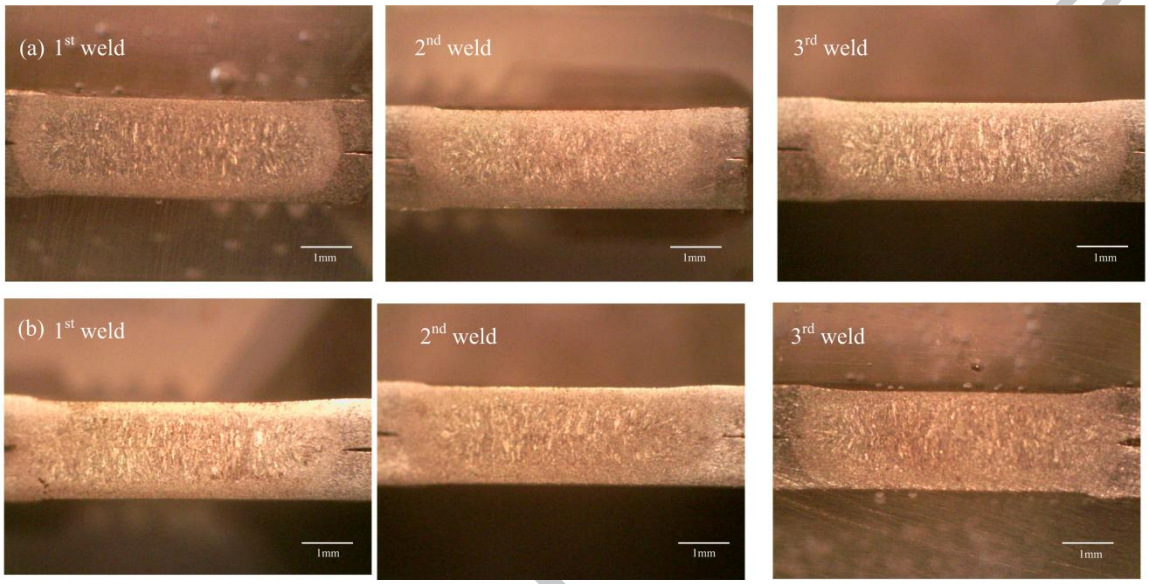

Figure 12 Longitudinal-sectional views of the double shunted welds made on a 1-mm mild steel, with weld spacing of (a) 8 mm and (b) 15 mm.

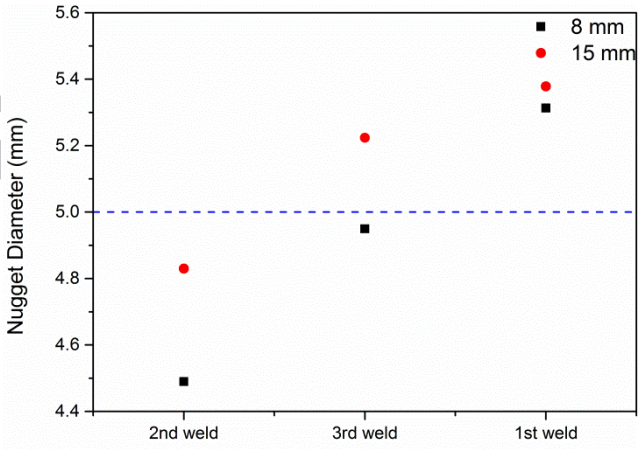

Figure 13 Nugget diameters of single shunting and double shunting

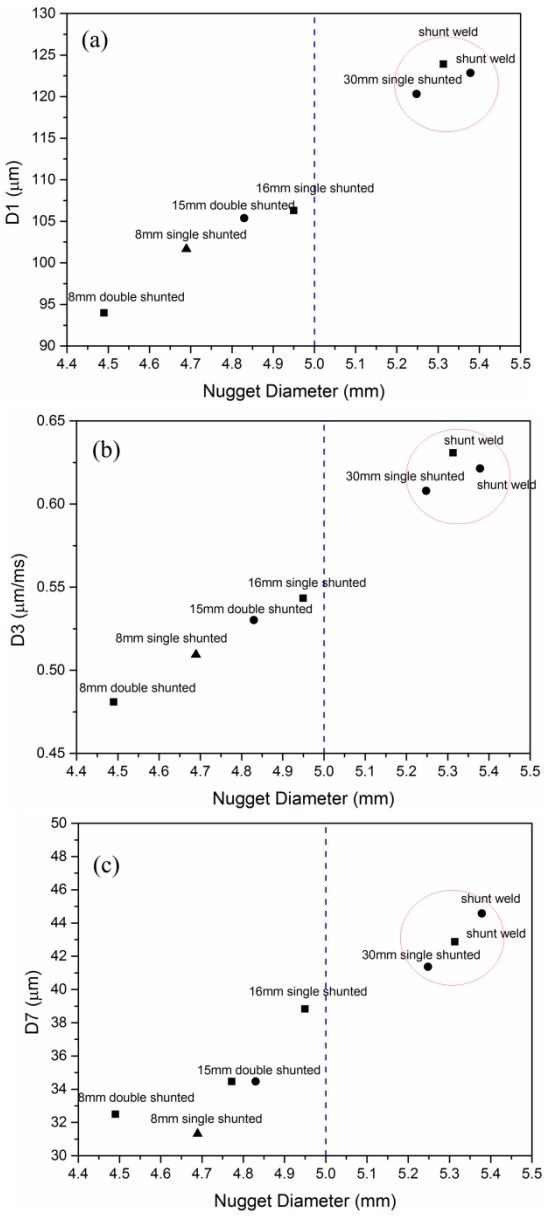

Figure 14 Profile quantities and nugget diameters with single and double shunting. (a) D1. (b) D3. (c) D7

Figure 14 summarises the relationship between the profile quantities and the measured nugget diameters under various shunting conditions. It is worth mentioning that D1, D3 and D7 can precisely predict the nugget diameter in double shunting at different weld spacing. Good linear correlations are held among extracted profile features and nugget diameters for the shunted weld. Welds with acceptable sized nugget are circled, which are well distinguished from shunted welds with undersized nugget. A double shunted weld generates much smaller nugget diameter than a single shunted weld at the same weld spacing. From equation (4), it is worth mentioning that the additional shunt weld diverts a substantial portion of the welding current and produces an undersized weld.

3.4 Comparison with dynamic resistance signal

Many existing studies have built weld quality monitoring systems based on dynamic resistance signals of the single weld [23,32,33]. They identified that, for the single weld, the dynamic resistance curve varies with respect to welding parameters and can be utilised for quality monitoring via its endpoint value and mean value. Spot welds with large nugget diameter usually have lower mean values and end point values than those with small nugget diameter. In this study, dynamic resistances with shunting were measured at different weld spacing ranging from 8 mm to 30 mm. The dynamic resistance signals of single shunted welds and double shunted welds are demonstrated in Figure 15 (a) and Figure 16 (a) and (b), respectively. For single shunted welds, the bulk resistance in shunting $R_{b,s}$ was proportional to weld spacing. The ratio $(R_{b,w} + R_{f,w})/ R_{b,s}$ declined under increased weld spacing. The dynamic resistances of shunted welds, equivalent to the total resistances in Figure 3 (b), tended to decrease with increased weld spacing, according to equation (6). As a consequence, DR curves were found to shift downward with the decline of weld spacing.

$$R=2R_{CE}+\frac{R_{b,s}\cdot(R_{b,w}+R_{f,w})}{R_{b,w}+R_{f,w}+R_{b,s}} \tag{6}$$

Similar to above characterisation on ED signal, the mean value of DR against weld spacing was firstly derived from the DR curves. The relationship between nugget diameter and the mean value of DR is established for the single shunted weld, as shown in Figure 15 (b) and (c), where strong correlations are found. Likewise, the mean value of DR in double shunting is illustrated in Figure 16 (c) and (d). It is notable that the contribution of the shunted path to total resistance has been doubled with two existing welds, making the associated DR curve to decline. The findings in the comparison for single shunting and double shunting validate that DR signals are affected by the additional parallel circuit caused by shunting. The existing quality monitoring system, established on DR signals of single welds, is found to make little contribution to characterising the quality of welds with severe shunting [23]. It is likely that inaccurate result on shunted weld can be yielded from DR signals.

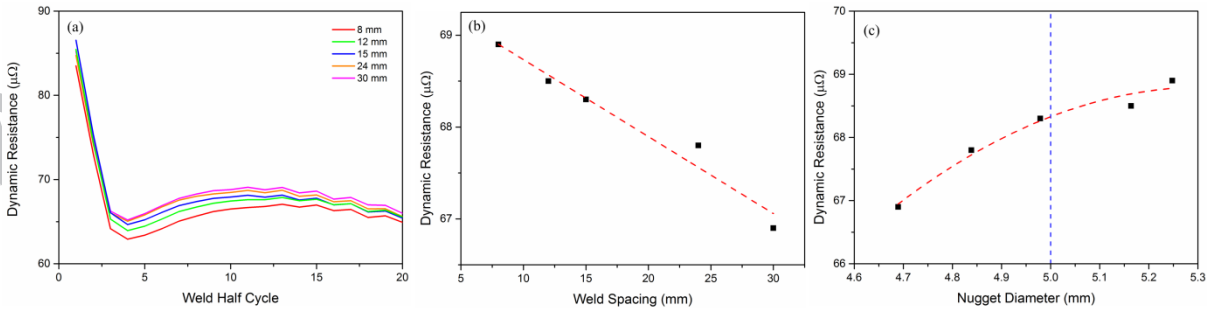

Figure 15 (a) Dynamic resistance of first shunted weld with different weld spacing. (b) Mean values of dynamic resistance at different weld spacing. (c) Mean values of dynamic resistance against nugget diameters.

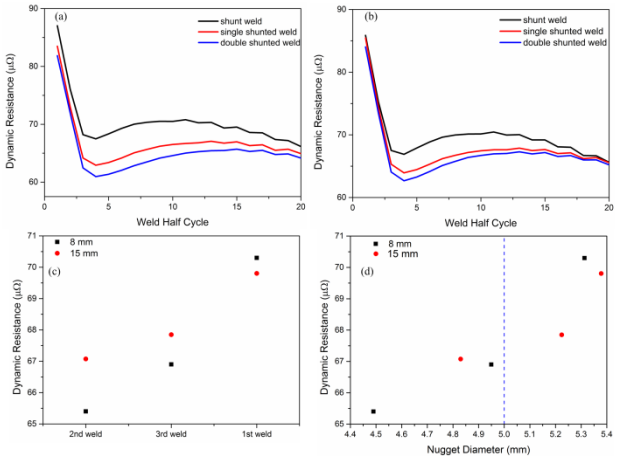

Figure 16 Dynamic resistance of double shunted welds with weld spacing of (a) 8 mm and (b) 15 mm. (c) Mean values of dynamic resistance in double shunting. (d) Mean values of dynamic resistance against nugget diameters.

4. Conclusion

The electrode displacement signals were used to characterise shunting problem in mild steel at different weld spacing and with multiple instances of shunt welds. Profile features including peak value and electrode displacement velocity were found for identifying minimum weld spacing of mild steel and undersized welds due to severe shunting. Double shunting increased diverted current along the shunt path, making the nugget diameter further shrink. Dynamic resistance signals suffering from shunting were found to be affected by the parallel circuit of shunting and welding path, which is contradictory to the trends established in the existing studies. Electrode displacement signal can better interpret shunting problem and can be incorporated into existing quality monitoring system constructed from single welds.

To alleviate the shunting effect in mild steel, increased welding current may be designated to compensate the heat input for the shunted weld. This method, however, results from a rise of the thermal expansion of the sheets and electrodes. A current control system can be adopted based on electrode displacement. Profile features extracted from shunt welds in this study are useful in determining the welding current to be increased. Furthermore, it is also important to understand the contribution of the electrodes to the thermal expansion under various process conditions, by comparing ED under image processing and displacement sensors. The nodal displacements on the centreline of the electrodes can predict the contribution of electrode expansion to total displacement via numerical simulation.

Acknowledgement:

The financial support from the Australian Research Council (Grant No. LP130101001) is fully acknowledged. The authors would like to thank Mr. Haiyang Zhou from ANU for providing the laser sensor. The authors would like to also thank Mr. Erasmo Scipione from ANU for providing technical assistance.

Reference

1. P. Podržaj, B. Jerman, S. Simončič, Poor fit-up condition in resistance spot welding, J. Mater. Process. Tech. 230 (2016) 21-25.
2. Y. Li, B. Wang, Q. Shen, M. Lou, H. Zhang, Shunting effect in resistance spot welding steels—part 2: theoretical analysis, Weld. J. 92 (2013) 231-238.
3. B. Wang, M. Lou, Q. Shen, Y. Li, H. Zhang, Shunting effect in resistance spot welding steels—part 1: experimental study, Weld. J. 92 (2013).
4. J. Bi, J. Song, Q. Wei, Y. Zhang, Y. Li, Z. Luo, Characteristics of shunting in resistance spot welding for dissimilar unequal-thickness aluminum alloys under large thickness ratio, Mater. Design. 101 (2016) 226-235.
5. Y. Li, J. Bi, Y. Zhang, Z. Luo, W. Liu, Shunting characteristics in triangular arranged resistance spot welding of dissimilar unequal-thickness aluminum alloys, Int. J. Adv. Manuf. Tech (2017) 1-8.
6. M. Jafari Vardanjani, A. Araee, J. Senkara, J. Jakubowski, J. Godek, Theoretical analysis of shunting effect in resistance spot welding (RSW) of AA2219, J. Chin. Inst. Eng. 39 (2016) 907-918.
7. H. Chang, H. Cho, A study on the shunt effect in resistance spot welding, Weld. J. 69 (1990) 308-316.
8. M. S. Choobi, C. Nielsen, N. Bayk, Finite Element and Experimental Study of Shunting in Resistance Spot Welding,Proceedings of the 11th International Seminar on Numerical Analysis of Weldability;(2015). pp. 27-30.
9. D. Browne, H. Chandler, J. Evans, P. James, J. Wen, C. Newton, Computer simulation of resistance spot welding in aluminum: Part II, Weld. J. 74 (1995).
10. P. Podržaj, I. Polajnar, J. Diaci, Z. Kariž, Overview of resistance spot welding control, Sci. Technol. Weld. Joi 13 (2008) 215-224.
11. Y. Ma, P. Wu, C. Xuan, Y. Zhang, H. Su, Review on techniques for on-line monitoring of resistance spot welding process, Adv. Mater. Sci. Eng. 2013 (2013).
12. S. Simončič, P. Podržaj, Resistance spot weld strength estimation based on electrode tip displacement/velocity curve obtained by image processing, Sci. Technol. Weld. Joi 19 (2014) 468-475.
13. S. Simončič, P. Podržaj, Image-based electrode tip displacement in resistance spot welding, Meas. Sci. Technol. 23 (2012) 065401.
14. P. Podržaj, S. Simončič, A machine vision-based electrode displacement measurement, WELD. WORLD. 58 (2014) 93-99.
15. L. Xinmin, Z. Xiaoyun, Z. Yansong, C. Guanlong, Weld quality inspection based on online measured indentation from servo encoder in resistance spot welding, IEEE. T. Instrum. Meas. 56 (2007) 1501-1505.
16. H. Wang, Y. Zhang, G. Chen, Resistance spot welding processing monitoring based on electrode displacement curve using moving range chart, Measurement 42 (2009) 1032-1038.
17. H. Zhang, F. Wang, T. Xi, J. Zhao, L. Wang, W. Gao, A novel quality evaluation method for resistance spot welding based on the electrode displacement signal and the Chernoff faces technique, Mech. Syst. Signal Pr. 62 (2015) 431-443.
18. C. Ji, Y. Zhou, Dynamic electrode force and displacement in resistance spot welding of aluminum, J. Manuf. Sci. Eng. 126 (2004) 605-610.
19. Y. Zhang, H. Shan, Y. Li, C. F. Zhao, Z. Luo, J. Guo, C. Y. Ma, Effects of the oxide film on the spot joining of aluminum alloy sheets: a comparative study between resistance spot welding and resistance spot clinching, Int. J. Adv. Manuf. Technol. (2017) 1-10.

20. M. Jou, Real time monitoring weld quality of resistance spot welding for the fabrication of sheet metal assemblies, J. Mater. Process. Tech. 132 (2003) 102-113.
21. Y. Zhang, H. Wang, G. Chen, X. Zhang, Monitoring and intelligent control of electrode wear based on a measured electrode displacement curve in resistance spot welding, Meas. Sci. Technol. 18 (2007) 867.
22. L. Wang, Y. Hou, H. Zhang, J. Zhao, T. Xi, X. Qi, Y. Li, A new measurement method for the dynamic resistance signal during the resistance spot welding process, Meas. Sci. Technol. 27 (2016) 095009.
23. J. Wen, C. Wang, G. Xu, X. Zhang, Real time monitoring weld quality of resistance spot welding for stainless steel, Isij Int. 49 (2009) 553-556.
24. X. Wang, Y. Li, G. Meng, Monitoring of resistance spot weld quality using electrode vibration signals, Meas. Sci. Technol. 22 (2011) 045705.
25. X. Hu, G. Zou, S. Dong, M. Lee, J. Jung, Y. Zhou, Effects of steel coatings on electrode life in resistance spot welding of galvannealed steel sheets, Mater. Trans. 51 (2010) 2236-2242.
26. B. Xing, Y, Xiao,, Q.H., Qin and H, Cui, Quality assessment of resistance spot welding process based on dynamic resistance signal and random forest based, Int. J. Adv. Manuf. Technol. (2017).
27. ISO 18278-2:2004, Resistance welding, Weldability, Part 2: Alternative procedures for the assessment of sheet steels for spot welding, 2004.
28. X. Wang, Y. Li, G. Meng, Monitoring of resistance spot weld quality using electrode vibration signals, Meas. Sci. Technol. 22 (2011) 045705.
29. Q. Fan, G. Xu, X. Gu, Expulsion characterization of stainless steel resistance spot welding based on dynamic resistance signal, J. Mater. Process. Tech. 236 (2016) 235-240.
30. X. Lai, X. Zhang, Y. Zhang, G. Chen, Weld quality inspection based on online measured indentation from servo encoder in resistance spot welding, IEEE. T. Instrum. Meas. 56 (2007) 1501-1505.
31. M. Pouranvari, S. Marashi, Factors affecting mechanical properties of resistance spot welds, Mater. Sci. Tech-lond. 26 (2010) 1137-1144.
32. Y. Luo, W. Rui, X. Xie, Y. Zhu, Study on the nugget growth in single-phase AC resistance spot welding based on the calculation of dynamic resistance, J. Mater. Process. Tech. 229 (2016) 492-500.
33. X. Wan, Y. Wang, D. Zhao, Quality monitoring based on dynamic resistance and principal component analysis in small scale resistance spot welding process, Int. J. Adv. Manuf. Tech (2016) 1-9.

Table of Figures

Table of Tables

Highlights:

- Electrode displacement is found to be sensitive to weld spacing in shunting
- Peak value and ED velocity can be used to determine the minimum weld spacing
- Dynamic resistance is tuned by the parallel circuit created by shunting path.